DOE/NASA/1028-79/2
NASA TM-79101

EVALUATION OF MOSTAS COMPUTER CODE FOR PREDICTING DYNAMIC LOADS IN TWO-BLADED WIND TURBINES

K. R. V. Kaza
The University of Toledo

and

D. C. Janetzke and T. L. Sullivan
National Aeronautics and Space Administration
Lewis Research Center

Work performed for
U.S. DEPARTMENT OF ENERGY
Office of Energy Technology
Division of Distributed Solar Technology

TECHNICAL PAPER to be presented at the
AIAA/ASME/ASCE/AHS Twentieth Structures,
Structural Dynamics, and Materials Conference
St. Louis, Missouri, April 4-6, 1979

NOTICE

DOE/NASA/1028-79/2
NASA TM-79101

EVALUATION OF MOSTAS COMPUTER CODE FOR PREDICTING DYNAMIC LOADS IN TWO-BLADED WIND TURBINES

K. R. V. Kaza
The University of Toledo
Toledo, Ohio 43606

and

D. C. Janetzke and T. L. Sullivan
National Aeronautics and Space Administration
Lewis Research Center
Cleveland, Ohio 44135

Prepared for
U. S. DEPARTMENT OF ENERGY
Office of Energy Technology
Division of Distributed Solar Technology
Washington, D. C. 20545
Under Interagency Agreement E(49-26)-1028

AIAA/ASME/ASCE/AHS Twentieth Structures,
Structural Dynamics, and Materials Conference
St. Louis, Missouri, April 4-6, 1979

EVALUATION OF MOSTAS COMPUTER CODE FOR PREDICTING DYNAMIC LOADS IN TWO-BLADED WIND TURBINES

K. R. V. Kaza,* D. C. Janetzke,**
and T. L. Sullivan**
National Aeronautics and Space Administration
Lewis Research Center
Cleveland, Ohio 44135

E-9925

Abstract

Calculated dynamic blade loads are compared with measured loads over a range of yaw stiffnesses of the DOE/NASA Mod-0 wind turbine to evaluate the performance of two versions of the MOSTAS computer code. The first version uses a time-averaged coefficient approximation in conjunction with a multiblade coordinate transformation for two-bladed rotors to solve the equations of motion by standard eigenanalysis. The results obtained with this approximate analysis do not agree with dynamic blade load amplifications at or close to resonance conditions. The results of the second version, which accounts for periodic coefficients while solving the equations by a time history integration, compare well with the measured data. To explain the deficiencies of the first version and to examine the validity of the transformation, an investigation was made with the aid of a hypothetical three-degree of freedom dynamic model. The exact equations of motion of this model were solved using the Floquet-Lipunov method both before and after applying the transformation. Next, the equations with time-averaged coefficients after applying the transformation were solved by standard eigenanalysis. It was found that the transformation is valid but the associated time-averaged coefficient approximation is inadequate for dynamic analysis of two-bladed rotors.

Nomenclature

a_1, b_1	multiblade coordinates of hypothetical model
B_1, B_2, B_3, B_4	power train damping constants
C_1, C_2, C_3, C_4	power train damping constants
I	blade mass moment of inertia of hypothetical model
I_{xx}, I_{yy}, I_{zz}	mass moment of inertias of pod
J_1, J_2, J_3, J_4	power train torsional inertias
K_1, K_2, K_3, K_4	power train stiffnesses
k	integer, 1, 2, 3, ...
K_t	equivalent linear spring of tower in the lateral direction of hypothetical model
K_ζ	equivalent rotational spring of blade in the edgewise direction
M	blade mass of hypothetical model
M_e	hypothetical model effective mass moving in the lateral direction which includes tower, bed plate, and generator
M_t	$M_e + 2M$
M_y	flatwise bending moment
m	blade mass per unit length of hypothetical model
n	integer, 1, 2, 3, ...
q	tower lateral degree of freedom of hypothetical model
R	radius of hypothetical model
r	hypothetical model blade coordinate
S	blade mass moment of hypothetical model
s	Laplace variable
X,Y	coordinate system of hypothetical model
X_p, X_p, X_p	coordinate system of pod
γ_g	generator torque
γ_r	torque applied to the rotor
δM_y	flatwise cyclic bending moment
ζ_o	multiblade coordinate of hypothetical model
ζ_1, ζ_2	lead-lag degrees of freedom of blades 1 and 2 of hypothetical model
σ	standard deviation
$\phi_1, \phi_2, \ldots \phi_5$	power train degrees of freedom
ϕ_n	blade phase angle of nth harmonic
ψ	azimuth angle
$\omega_1, \omega_2, \omega_3$	coupled frequencies of hypothetical model in the fixed coordinated system
$\omega_{f_1}, \omega_{f_2}, \omega_{f_3}$	frequencies of Floquet transition matrix
ω_t	tower lateral frequency of hypothetical model
ω_ζ	blade lead-lag frequency of hypothetical model
Ω	rotational speed of rotor
$(\dot{})$	time derviative
$( )'$	derivative with respect to ψ
[ ]	square matrix
{ }	column matrix
$[\ ]^T$	transpose of a matrix

Introduction

The analytical calculation of rotor blade loads is one of the most difficult problems in both rotary wing technology and horizontal axis wind turbine technology, since it involves solving a highly nonlinear dynamic response problem. In Ref. 1 several analytical methods for calculating loads on a hypothetical helicopter rotor were compared. In Ref. 2 seven computer codes for calculating dynamic loads in horizontal axis wind turbines were compared on the basis of calculated loads, with steady state measured data as a standard. One of the codes evaluated in Ref. 2 is MOSTAS,[3] a code developed for NASA by Paragon Pacific, Inc. (PPI) to calculate dynamic loads and stability in a complete horizontal axis wind turbine system. That evaluation of MOSTAS was of a preliminary nature.

*Adjunct Associate Professor of Mechanical Engineering, The University of Toledo, Toledo, Ohio, Member AIAA.
**Research Engineer, Wind Energy Project Office.

AIAA Paper No. 79-0733

More recently the scope of MOSTAS has been extended to account for time varying coefficients in the governing equations of motion of the wind turbine system. For descriptive purposes, the earlier version of MOSTAS will be designated herein as MOSTAS-A and the extended version as MOSTAS-B.

The objective of this study is to conduct an indepth evaluation of the MOSTAS-A and -B codes to determine their suitability for predicting dynamic loads and instabilities in two-bladed wind turbines. This evaluation was accomplished by comparing blade loads measured on the DOE/NASA Mod-0 wind turbine against the load predictions of the two codes. The Mod-0 wind turbine, shown in Fig. 1, is an experimental 100 kW horizontal axis machine which was designed and built as a part of the DOE/NASA wind energy program and is now in operation at the NASA Plum Brook Station near Sandusky, Ohio.[4]

For the purpose of comparison, blade loads are chosen because of their importance in the design of large rotor systems. Since the dynamic coupling between the rotor and the tower and resulting dynamic blade loads are sensitive to the variations in yaw stiffness, the loads for different values of yaw stiffness are compared. With the help of these results the performance of both versions of the MOSTAS code for predicting dynamic loads was evaluated. This evaluation raised some questions regarding the validity of two major assumptions used for two-bladed rotors in MOSTAS-A. These assumptions for calculating system frequencies, dynamic loads, and dynamic stability for two-bladed rotors are that the results are not affected either by the use of a multiblade coordinate transformation[5] or by the use of time-averaged coefficient approximation (approximate method). To assess the validity of these assumptions an additional study was performed with the aid of a simple hypothetical mathematical model. This paper presents results of both the load comparison study and the hypothetical model study.

Description of MOSTAS-A and -B Codes

The MOSTAS code is a collection of programs, beginning with a rotor code called MOSTAB-HFW in which the flexibility of each blade can be represented by one to four modes. The support of the rotor is assumed to be rigid. Details of the -HFW code are given in Ref. 6. MOSTAS-HFW prints the key results of the trim-search process and also generates two disk or tape data files to be processed by subcodes PROCES and ROLIM. PROCES performs a harmonic analysis of the blade loads and ROLIM forms the rotor model from the single blade linear math model produced by -HFW. During this process ROLIM uses a multiblade coordinate transformation for a two-bladed rotor described in Ref. 5 and synthesizes a rigorous linear rotor model in periodic coefficients.

Unlike the multiblade coordinate transformation for rotors with three or more blades,[7] the transformation for two-bladed rotors assumes a constraint relation between the multiblade coordinates. The effect of these transformations on the equations of motion is to remove from the coefficients the harmonic terms which are not the integer multiples of number of blades.

The ROLIM linear rotor model is combined with linear models of other components of the wind turbine system to produce a coupled system model. The coupling program is called WINDLASS. WINDLASS has provision for five different elements of the wind turbine system: rotor, control system, power train, pod, and tower. In the process of coupling, all periodic terms in the coefficients in the rotor model are time-averaged over one period so that the resulting equations for stability can be solved by standard eigenanalysis. The corresponding method of solution is referred to herein as the approximate method.

The dynamic response of the coupled wind turbine system to harmonic loads is processed by two subcodes, DYNAM2 and RECOV2. DYNAM2 calculates the frequency response to harmonic loads and RECOV2 calculates time history response. The total dynamic loads are obtained by adding MOSTAB-HFW fixed-shaft loads and perturbation loads from RECOV2. The version of the MOSTAS code obtained by combining the programs MOSTAB-HFW, ROLIM, WINDLASS, DYNAM2, and RECOV2 is referred to as MOSTAS-A.

The MOSTAS-A code was extended to include all periodic coefficients in the equations of motion and to handle the arbitrary time varying loads by adding another program called WINDGUST,[8] in which the equations with periodic coefficients are integrated numerically. WINDGUST replaces the programs DYNAM2 and RECOV2. From the time history response, the total dynamic loads are obtained by adding MOSTAS-HFW fixed-shaft loads and the perturbation loads. This version of the system code is referred to as MOSTAS-B.

Description of Mod-0 Wind Turbine

The Mod-0 wind turbine is shown in Fig. 1. The system consists of five main components which are the rotor, the control system, the power train, the pod, and the tower. The rotor operates at 40 rpm, generating 100 kW of electric power in an 18 mph wind. The two aluminum blades are attached through pitch bearings to a rigid hub which is connected by means of a low speed shaft to a 45:1 step-up gear box. A high speed shaft (1800 rpm) connects the gear box to the 100 kW synchronous generator. The power train assembly is contained within a pod which is mounted on top of a 93 foot steel truss tower. Yaw control allows alignment of the rotor axis with the wind direction. The rotor is located downwind of the tower. A brief description of the mathematical models of the various components used in the MOSTAS code is given in Appendix A.

Results and Discussion

Experimental Data

Bending moments measured in the shank area of the Mod-0 blades (5% of span) are used to evaluate the load prediction-capabilities of the MOSTAS-A and MOSTAS-B codes. Selected load data are divided into two groups, as follows:

1. Data Case I. Data Case I was defined in Ref. 2 for purposes of comparing and validating wind turbine computer codes. This case represents the response of the Mod-0 wind turbine in its initial configuration, with stairs in the tower and a single

yaw drive unit connecting the pod to the tower. The nominal wind speed at rotor hub height is 28 mph. Complete time histories of load are available for this case. Data Case I is characterized by high blade loads and substantial rotor/tower interaction.

2. Variable yaw-stiffness data. The effect of yaw stiffness on blade loads was measured by changing the yaw drive system to the following configurations: (1) free yaw, in which the yaw drive was disconnected completely; (2) single yaw drive, (3) dual yaw drive, consisting of two parallel single yaw drive systems; (4) dual yaw drive with preload, in which backlash and nonlinearity were removed from the dual yaw drive system by loading the two systems against one another to a level of about 30,000 lb-in; and (5) fixed yaw drive, in which the pod was clamped to the tower by brakes. In all cases the wind speed was approximately 25 mph and there were no stairs in the tower, the latter having been removed permanently to reduce tower shadow loads on the blades.

Blade Load Comparison for Data Case I

Because of its pronounced response, Data Case I is chosen for an indepth comparison of experimental and analytical data. Figure 2 shows time histories of experimental and analytical blade bending moments in both flatwise and edgewise directions for this case. The abscissa is the blade azimuth angle which is 0^{o} and 360^{o} when the blade points downward. The flatwise bending moment is positive if the blade bends into the wind; the edgewise bending moment is positive if the leading edge is in tension. The experimental time histories are presented as a band whose upper and lower bounds enclose data for three consecutive cycles. These data were also presented in Ref. 2.

The comparison in Fig. 2(a) shows that the maximum and minimum flatwise bending moments predicted by both MOSTAS-A and -B codes are almost equal. However, MOSTAS-A results show four peaks per cycle and those of MOSTAS-B show three peaks. Measured maximum and minimum values are smaller in magnitude than those of either code. Measured data show three peaks and the amplitude of these peaks decreases at a much faster rate than that predicted by either code. This conservative nature of the calculated flatwise loads may be the result of the following factors: (1) the assumption that the structural damping of the yaw drive system is zero, (2) the differences between the actual and analytical values of tower shadow and wind shear, and (3) the nonlinear behavior of the actual yaw drive system. The first factor is probably the most significant. Some efforts to account for the damping of the yaw drive system are being made.

The edgewise load comparison in Fig. 2(b) shows that the time history of moment predicted by MOSTAS-A significantly differs from that of MOSTAS-B. The measured time history of moment is in agreement with that predicted by MOSTAS-B except for a slight difference in phase angle. The maximum and minimum moments predicted by means of MOSTAS-A are smaller than those obtained with MOSTAS-B.

Table 1 presents a comparison between measured and calculated data on the basis of maximum, minimum, steady and cyclic bending moments. These results quantify the comparisons in Fig. 2. The steady ($\overline{M}_y$) and cyclic (δM_y) flatwise bending moments are defined by the following equations:

$$\overline{M}_y = \frac{1}{2}\left(M_{y,max} + M_{y,min}\right) \tag{1}$$

$$\delta M_y = \frac{1}{2}\left(M_{y,max} - M_{y,min}\right) \tag{2}$$

where $M_{y,max}$ and $M_{y,min}$ are the extreme values of flatwise bending moments during one revolution. Similar equations apply for edgewise bending moments.

Examination of Table 1 shows that correlation between measured and calculated bending moments is highly variable. Good correlation was achieved between measured edgewise moments and MOSTAS-B predictions. All other comparisons show generally poor correlation.

To compare the measured and calculated data on the basis of harmonic content, the bending moments shown in Fig. 2 are expressed in the following Fourier Series:

$$\delta M = \sum_{n} C_n \sin(n\psi + \phi_n) \qquad n = 0,1,2,\ldots \tag{3}$$

where δM is the cyclic moment load in lb-ft, C_n is the amplitude of the nth harmonic in the lb-ft, ψ is the azimuth angle of the blade, and ϕ_n is the phase angle of the nth harmonic. Table 2 contains measured and calculated values of harmonic data for Data Case I. The measured amplitudes and phase angles are taken from Ref. 2 and these are averages of the bounding values. For further comparison purposes, each harmonic amplitude was normalized with respect to its cyclic load. These normalized measured and calculated values are compared in Fig. 3. The comparison shows that the measured harmonic amplitudes continually decrease with increasing number except the fourth and fifth harmonics in the edgewise direction and the third harmonic in the flatwise direction. The correlation between the measured and calculated harmonic amplitudes varies from very poor to very good depending upon the harmonic number.

In summary, Data Case I load comparisons were inconclusive as to the validity of MOSTAS-A and -B codes. Correlation was highly variable, with MOSTAS-B correlation being some what better than that of MOSTAS-A.

Blade Load Correlation for Variable Yaw Stiffness

Because of the importance of the cyclic bending moments for predicting life of blades and because of the sensitivities of the blade loads to the variations in yaw stiffness, the experimental and analytical cyclic bending moments are compared for different values of yaw stiffness in Fig. 4. The abscissa is the effective yaw stiffness which is the resultant of the torsional stiffnesses of the tower and the yaw drive system in series. The measured median cyclic bending moments together with 16th and 84th percentiles are shown in Fig. 4. The band between the 16th and 84th percentiles approximates a $\pm 1\sigma$ band and contains the loads for 68 percent of the rotor revolutions.

The comparison of cyclic flatwise bending moments in Fig. 4(a) shows that both the MOSTAS-A and -B calculated loads are generally larger than the measured loads. MOSTAS-B predicts dynamic load magnifications whenever a nonrotating system frequency is close to an even integer multiple of the rotor rotational frequency. These magnifications in loads should be present because the entire wind turbine system as observed in the nonrotating coordinate system is subjected to zeroth, second, fourth, and sixth harmonic loads generated by the rotor. In particular, the magnification predicted by MOSTAS-B due to 2/rev resonance involving predominently yaw motion is in good agreement with the magnification observed in the Mod-0 wind turbine with a single yaw drive and a dual yaw drive without preload. Although the flatwise loads predicted by MOSTAS-A for single yaw and dual yaw drive stiffnesses are higher than those of experiment, the load variation with yaw stiffness close to these cases is not in agreement with measured values. Also, the MOSTAS-A code is unable to predict expected dynamic load amplifications when the nonrotating system frequencies are 4/rev and 6/rev. The MOSTAS-B code does predict these resonances.

The comparison of edgewise bending moments in Fig. 4(b) shows that both MOSTAS-A and -B code values are in agreement with the measured values for the free yaw, preloaded dual yaw, and fixed yaw cases in which the system is free from resonance. The edgewise moments predicted using the MOSTAS-A code for the single yaw drive and the dual yaw drive without preload are not in agreement with measured values. MOSTAS-B loads, however, are in good agreement with measured loads for these yaw stiffnesses near the 2/rev resonance. The lack of correlation between measured and MOSTAS-A cyclic flatwise and edgewise bending moments at or close to the 2/rev resonance clearly indicates deficiencies in this version of the code.

Evaluation of Codes for Dynamic Load Predictions

Based on the comparisons in the preceeding sections, it is inferred that the MOSTAS-A code, which uses an approximate method (time-averaged coefficients) in conjunction with a multiblade coordinate transformation is inadequate for predicting dynamic load amplifications in two-bladed rotors. The MOSTAS-B code, which also uses the multiblade coordinate transformation but accounts for periodic coefficients, predicts dynamic amplifications in agreement with measured values. Comparison of the two codes and measured data on the basis of harmonic amplitudes is inconclusive.

The apparent cause of the poor performance of the MOSTAS-A code is the time-averaged coefficient approximation, which was introduced so that eigenanalysis could be used to solve the system equations of motion. The multiblade coordinate transformation, on the other hand, appears to be valid since it is also used in the MOSTAS-B code which was found to yield valid load predictions. In order to test these two hypotheses--that the time-averaged coefficient approximation is invalid for two-bladed rotors and that the multiblade transformation is valid--a study was conducted by means of a hypothetical two-bladed wind turbine model with three degrees of freedom. Details of this study are given in Appendix B.

As shown in Appendix B, calculation of system frequencies by means of accepted Floquet theory[7,9,10,13] is unaffected by the multiblade transformation. However, the time-averaged coefficient approximation which is used in the MOSTAS-A code alters system frequencies so that they do not agree with the exact Floquet frequencies. In particular, a condition of "ground resonance" in which two system frequencies are equal was predicted by the Floquet theory before and after applying the multiblade coordinate transformation but not by the approximate method. Thus, the hypothetical model study supports both hypotheses: (1) the multiblade coordinate transformation for two-bladed rotors is valid, and (2) the time-averaged coefficient approximation which is used in the MOSTAS-A code is invalid.

Conclusions

An investigation was performed to evaluate the validity of the MOSTAS-A and -B computer codes for predicting dynamic loads and instabilities in two-bladed wind turbines. This investigation was conducted with the aid of Mod-0 wind turbine data and the theoretical dynamic behavior of a hypothetical wind turbine model with three degrees of freedom. The following principal conclusions are drawn from the results obtained:

1. The MOSTAS-A code is invalid for predicting either loads or instabilities in two-bladed wind turbines.

2. The MOSTAS-B code is valid for predicting dynamic loads in two-bladed wind turbines. Good correlation between calculated and measured blade bending loads can be expected for systems like the Mod-0 wind turbine generator.

3. The cause of deficiencies in the MOSTAS-A code is the time-averaged coefficient approximation introduced to permit solution of the system equations of motion by eigenanalysis.

4. The multiblade transformation used in both codes and its constraint relation do not affect system frequencies and can be used for analyzing two-bladed rotors.

Appendix A

Component Models of Mod-0 Wind Turbine

For the purpose of analysis, the Mod-0 wind turbine is divided into five main components. The mathematical models for these individual components are described below.

1. Rotor model. The rotor has two metal blades, each 62.5 feet long and weighing 2000 pounds. The flexibility of each rotor blade is represented by a modal model which is defined as a series of blade mode shapes and frequencies along with a definition of mass properties. These properties are listed in Table 3. The blade aerodynamic forces are generated using "quasi-steady" blade element theory. The effects of gravity, the wind shear caused by the boundary layer of the Earth, and the tower shadow caused by rotor/tower aerodynamic interference are included. The wind shear is assumed to cause a 30 percent linear increase in wind speed

from the lowest to the highest point in the rotor disk. The tower shadow effect is considered by retarding the free-stream velocity in 15° sectors on either side of the tower center line. The amount of retardation used is 50 percent of nominal wind speed for the tower with stairs and 27 percent for tower without stairs, based on wind tunnel test data in Ref. 11.

2. Control system model. The pitch control system model used in this study is of first order as shown in Fig. 5(a). Also included in the control system is the model for the synchronous generator, Fig. 5(b), which is represented by a spring and a damper. Through this model, the generator torque is applied to the power train and the reaction is applied to the pod.

3. Power train model. The power train model is composed of a series of one-degree of freedom models, each representing a flexible shaft with rigid pinion and main gears at its ends. A schematic of the power train model of Mod-0 is shown in Fig. 6 and the properties of various components are listed in Table 4.

4. Pod model. The pod model is essentially an interfacing device for the other wind turbine components. It is assumed to be an elastic body with a concentrated mass. The elastic pod model is made up of three beam elements, as shown in Fig. 7, and its mass is concentrated at grid point 2. The mass properties are given in Table 5(a). The symmetric stiffness matrix K_p of this model (of order 24x24) was generated using standard engineering beam elements. The nonzero matrix elements on the diagonal and in the upper triangle are listed in Table 5(b). This stiffness matrix is compatible with an ordered vector (24x1) of pod grid point deflections resolved to pod inertial axes, shown in Fig. 7. The first six elements of the deflection vector represent three translations and three rotations for grid point 1, the next six for grid point 2, and so on. The pod also includes the yaw drive system which is represented by concentrated springs. The torsional stiffness of the yaw drive system is the major structural parameter which was varied during this study. The stiffness values used in the analytical calculations are listed in Table 5(c). The Mod-0 wind turbine yaw drive stiffness for the data cases addressed herein are given in Table 5(d).

5. Tower. The tower is represented by a series of mode shapes and frequencies along with a definition of its mass properties. The model properties of the tower were generated using the finite element structural analysis program NASTRAN. In calculating the modes and frequencies of the tower as an isolated component, a concentrated mass and mass moment of inertia were placed at the top of the tower to approximate the mass properties of the pod, rotor, power train, and generator system. Then, when all the modules of the system were coupled together, the concentrated mass and mass moment of inertia were removed. By this approach a better representation of the tower mass and elastic characteristics is achieved with fewer number of tower modes. A total of three modes, one lateral bending, one fore and aft bending, and one torsion mode, were used for the tower model. The properties of these modes are listed in Table 6.

Appendix B

Hypothetical Three-Degree Freedom Model

The purpose of the hypothetical model, as stated earlier, is to assess the validity of the multiblade coordinate transformation for two-bladed rotors and the associated time-averaged coefficient approximation (approximate method) which is used in MOSTAS-A code. To this end, a very simple model with two blades is considered, in order, to minimize the complexity associated with the Floquet-Liapunov theory which will be used to solve the equations of motion with periodic coefficients. The aerodynamic and gravitional forces are not included. The degrees of freedom of this model are the tower lateral motion and blade lead-lag motion. The tower is represented by an "equivalent" mass and a linear spring, and each blade is assumed to be rigid. The flexibility of the blade in the lead-lag direction is concentrated at the hinge which is assumed to be on the axis of rotation. A schematic of this model is shown in Fig. 8.

The development of the equations of motion for this model is a straight forward application of Hamilton's principle.[12] Without the derivation details, these equations are as follows:

$$\left.\begin{aligned} &M_t\ddot{q} + K_t q + S(\zeta_1 \cos\psi - \zeta_2 \cos\psi)^{\cdot\cdot} = 0 \\ &I\ddot{\zeta}_1 + K_\zeta \zeta_1 + S\ddot{q}\cos\psi = 0 \\ &I\ddot{\zeta}_2 + K_\zeta \zeta_2 - S\ddot{q}\cos\psi = 0 \end{aligned}\right\} \quad \text{(B1)}$$

where

$$\left.\begin{aligned} M &= \int_0^R m\,dr \\ S &= \int_0^R mr\,dr \\ I &= \int_0^R mr^2\,dr \\ M_t &= M_e + 2M \end{aligned}\right\} \quad \text{(B2)}$$

and M_e is the effective mass in the lateral direction which includes both the tower and the pod.

For convenience, the above equations are nondimensionalized and expressed in the state vector form

$$[P]\{u'\} - [Q]\{u\} = 0 \quad \text{(B3)}$$

where

$$[P] = \begin{bmatrix} 1 & 0 & 0 & 0 & 0 & 0 \\ 0 & 1 & 0 & \frac{S}{M_t R}\cos\psi & 0 & \frac{-S}{M_t R}\sin\psi \\ 0 & 0 & 1 & 0 & 0 & 0 \\ 0 & \frac{SR}{I}\cos\psi & 0 & 1 & 0 & 0 \\ 0 & 0 & 0 & 0 & 1 & 0 \\ 0 & \frac{-SR}{I}\cos\psi & 0 & 0 & 0 & 1 \end{bmatrix}.$$

$$[Q] = \begin{bmatrix} 0 & 1 & 0 & 0 & 0 & 0 \\ -\gamma_t^2 & 0 & \frac{S}{M_t R}\cos\psi & \frac{2S}{M_t R}\sin\psi & \frac{-S}{M_t R}\cos\psi & \frac{-2S}{M_t R}\sin\psi \\ 0 & 0 & 0 & 1 & 0 & 0 \\ 0 & 0 & -\gamma_\zeta^2 & 0 & 0 & 0 \\ 0 & 0 & 0 & 0 & 0 & 1 \\ 0 & 0 & 0 & 0 & -\gamma_\zeta^2 & 0 \end{bmatrix}$$

$$\{u\} = \left\{\frac{q}{R} \quad \frac{s}{R} \quad \zeta_1 \quad \zeta_1' \quad \zeta_2 \quad \zeta_2'\right\}^T$$

$$\gamma_t^2 = \frac{K_t}{M\Omega^2} = \frac{\omega_t^2}{\Omega^2}; \quad \gamma_\zeta^2 = \frac{K_\zeta}{L\Omega^2} = \frac{\omega_\zeta^2}{\Omega^2}$$

$$\frac{d(\,)}{dt} = \Omega \frac{d(\,)}{d\psi} = \Omega(\,)' \qquad \text{(B4)}$$

The multiblade coordinate transformation for two-bladed rotors was developed in Ref. 5 and it is given by the relation

$$\begin{Bmatrix} \zeta_1 \\ \zeta_1' \\ \zeta_2 \\ \zeta_2' \end{Bmatrix} = \begin{bmatrix} 1 & 0 & \cos\psi & \sin\psi \\ 0 & 1 & -\sin\psi & \cos\psi \\ 1 & 0 & -\cos\psi & -\sin\psi \\ 0 & 1 & \sin\psi & -\cos\psi \end{bmatrix} \begin{Bmatrix} \zeta_o \\ \zeta_o' \\ -a_1 \\ -b_1 \end{Bmatrix} \qquad \text{(B5)}$$

The effect of this transformation on Eq. (B3) is the absence of first harmonic terms in the coefficients and this effect is similar to the one exhibited by the multiblade transformation for rotors with three or more blades.[10] The above transformation, however, assumes a constraint relation between the multiblade coordinates a_1 and b_1 and it is (from Eq. (B5))

$$a_1' \cos\psi + b_1' \cos\psi = 0 \qquad \text{(B6)}$$

Combining the Eqs. (B3), (B4), and (B5), the resulting equations in the multiblade coordinates can be obtained and these are

$$[A]\{\zeta'\} - [B]\{\zeta\} = 0 \qquad \text{(B7)}$$

where

$$\{\zeta\} = \{u_1 \quad u_2 \quad \zeta_o \quad \zeta_o' \quad -a_1 \quad -b_1\}^T$$

$$[A] = \begin{bmatrix} 1 & 0 & 0 & 0 & 0 & 0 \\ 0 & 1 & 0 & 0 & \frac{-S}{M_t R}\sin 2\psi & \frac{S}{M_t R}(1+\cos 2\psi) \\ 0 & 0 & 1 & 0 & 0 & 0 \\ 0 & 0 & 0 & 1 & 0 & 0 \\ 0 & \frac{-SR}{I}\sin 2\psi & 0 & 0 & 1 & 0 \\ 0 & \frac{SR}{I}(1+\cos 2\psi) & 0 & 0 & 0 & 1 \end{bmatrix}$$

$$[B] = \begin{bmatrix} 0 & 1 & 0 & 0 & 0 & 0 \\ -\zeta_t^2 & 0 & 0 & 0 & \frac{-4S}{M_t R}\cos 2\psi & \frac{4S}{M_t R}\sin 2\psi \\ 0 & 0 & 0 & 1 & 0 & 0 \\ 0 & 0 & -\gamma_\zeta^2 & 0 & 0 & 0 \\ 0 & 0 & 0 & 0 & \frac{-\sin 2\psi}{2}(1-\gamma_\zeta^2) & \frac{(\gamma_\zeta^2-1)}{2} + \frac{\cos 2\psi}{2}(1-\gamma_\zeta^2) \\ 0 & 0 & 0 & 0 & \frac{(1-\gamma_\zeta^2)}{2} + \frac{(1-\gamma_\zeta^2)}{2}\cos 2\psi & \frac{\sin 2\psi}{2}(1-\gamma_\zeta^2) \end{bmatrix}$$

(B8)

The tower motion in Eqs. (B3) and (B7) is in the fixed-coordinate system, and the blade motions are in the rotating-coordinate system in Eq. (B3) and in the fixed-coordinate system in Eq. (B7). If the multiblade coordinate transformation is valid, the system frequencies obtained from Eqs. (B3) and (B7) must be equal when all the frequencies are expressed in either the fixed or rotating-coordinate system.

To check this equality in frequencies, Eqs. (B3) and (B7) were solved using the Floquet-Liapunov theory for various values of rotor speed. Since the frequencies obtained from this theory are indeterminant, one has to add an integer multiple of the basic frequency[7] to each frequency obtained from the Floquet Transition Matrix.[7] Thus, the frequencies of Eq. (B3) and the frequencies of the Floquet Transition Matrix of Eq. (B3) are related by the equation

$$\frac{\omega_i}{\Omega} = \frac{\omega_{f_i}}{\Omega} + k \qquad \begin{matrix} i = 1,2,3 \\ k = 1,2,3,\ldots \end{matrix} \qquad \text{(B9)}$$

Where ω_1, ω_2, and ω_3 are the rotor collective, the rotor cyclic, and the tower frequencies, respectively; ω_{f_i} are the corresponding frequencies of the Floquet Transition Matrix. The basic frequency for Eq. (B3) is 1/rev. The rotor frequencies in Eq. (B9) are in the rotating-coordinate system. For a later comparison, these rotor frequencies are expressed in the fixed-coordinate system and are tabulated together with the tower frequency in Table 7. It should be mentioned the system frequencies of Eq. (B3) are in agreement with the results presented in Ref. 13.

The frequencies of Eq. (B7) and the frequencies of the Floquet Transition Matrix of Eq. (B7) are related by the equation

$$\frac{\omega_i}{\Omega} = \frac{\omega_{f_i}}{\Omega} + 2k \qquad \begin{matrix} i = 1,2,3 \\ k = 1,2,3,\ldots \end{matrix} \qquad \text{(B10)}$$

The basic frequency for Eq. (B7) is 2/rev. The frequencies ω_1, ω_2, and ω_3 of Eq. (B7) are in the fixed-coordinate system. These are also included in Table 7.

Comparison of the frequencies of Eqs. (B3) and (B7) in Table 7 shows that the multiblade coordinate transformation does not effect the frequencies. Hence, the transformation can be used for two-bladed rotors.

To check the validity of the time-averaged coefficient approximation used in MOSTAS-A code, Eq. (B7) after approximating the periodic coefficients in Eq. (B8) was solved by a standard eigenanalysis method. The resulting frequencies are also tabulated in Table 7 under the heading "Approximate method."

The frequencies tabulated in Table 7 are also plotted in Fig. 9 where the variation of nondimensional system frequencies as a function nondimensional rotor speed is shown with nondimensional tower frequency as a parameter. Several interesting observations follow from the results. These are: (1) for rotational speed ratios Ω/ω_ζ between 0.2 and 0.4, the agreement between the Floquet and approximate method frequencies is rather poor, (2) for rotational speeds ratios between 2.2 and 2.6 the Floquet theory predicts the possibility of a ground resonance instability but the approximate method does not. Ground resonance is a phenomena characterized by the coalescence of two system frequencies and by the positive value of the real part of the eigenvalue. The Mod-0 wind turbine operates

in the rotational speed ratio range in which the agreement between the Floquet and approximate method frequencies is poor. These observations clearly suggests that the approximate method which is used in MOSTAS-A is not adequate to predict either the coupled frequencies or the possibility of ground resonance phenomena and hence any other dynamic instabilities.

References

1. Ormiston, R. A., "Comparison of Several Methods for Predicting Loads on a Hypothetical Helicopter Rotor," in Rotorcraft Dynamics, NASA SP-352, 1974, pp. S6-S24.

2. Spera, D. A., "Comparison of Computer Codes for Calculating Dynamic Loads in Wind Turbines," DOE/NASA/1028-78/16, NASA TM-73773, 1977.

3. Hoffman, J. A., "Coupled Dynamic Analysis of Wind Energy Systems," NASA CR-135152, 1977.

4. Puthoff, R. L., "Fabrication and Assembly of ERDA/NASA 100-Kilowatt Experimental Wind Turbine," NASA TM X-3390, 1976.

5. Hoffman, J. A., "A Multi-blade Coordinate Transformation Procedure for Rotors with Two Blades," Paragon Pacific, Inc., PPI-1014-5, Sep. 1976.

6. Henninger, W. C., Hoffman, J. A., and Williamson, D. R., "Wind Energy System Coupled Dynamics Analysis (MOSTAS): User's Manual," Paragon Pacific, Inc., PPI-1014-8/1014-9, Jan. 1977.

7. Hohenemser, K. H., and S.-K. Yin, "Some Applications of the Method of Multi-blade Coordinates," Journal of the American Helicopter Society, Vol. 17, No. 3, July 1972, pp. 3-12.

8. Williamson, D. R., Hoffman, J. A., and Henninger, W. C., "Mathematical Methods Incorporated in the Wind Energy System Coupled Dynamic Analysis," Paragon Pacific, Inc., PPI-1018-7, Sep. 1977.

9. Hammond, C. E., "An Application of Floquet Theory to Prediction of Mechanical Instability," Journal of American Helicopter Society, Vol. 19, No. 4, Oct. 1974, pp. 14-23.

10. Kaza, K. R. V., and Hammond, C. E., "An Investigation of Flap-Lag Stability of Wind Turbine Rotors in the Presence of Velocity Gradients and Helicopter Rotors in Forward Flight," in 17th Structures, Structural Dynamics and Materials Conference, American Institute of Aeronautics and Astronautics, New York, 1976, pp. 421-431.

11. Savino, J. M., and Wagner, L. H., "Wind Tunnel Measurements of the Tower Shadow on Models of the ERDA/NASA 100-kW Wind Turbine Tower," NASA TM X-73548, 1976.

12. Bisplinghoff, R. L., and Ashley, H., "Principles of Aeroelasticity," Wiley, New York, 1962.

13. Miller, R., Dugundji, J., Chopra, I., Sheu, D., and Wendell, J., "Wind Energy Conversion, Volume III: Dynamics of Horizontal Axis Wind Turbines," MIT Aeroelastic and Structures Research Laboratory, ASRL TR-184-9.

TABLE 1. - COMPARISON OF MEASURED AND CALCULATED BLADE LOADS FOR DATA CASE I

(a) Flatwise loads

Component	Bending moment, ft-lb		
	Measured	MOSTAS-A	MOSTAS-B
Max	127 500	161 200	153 000
Min	-2 500	-46 000	-42 000
Steady	62 500	57 600	55 500
Cyclic	±65 000	±103 600	±97 500

(b) Edgewise loads

Max	34 500	19 700	34 000
Min	-76 500	-54 500	-81 800
Steady	-21 000	-17 400	23 900
Cyclic	±55 500	±37 100	±57 900

TABLE 2. - HARMONIC CONTENT OF DATA CAST I BENDING LOADS AT STATION 40 (5% SPAN)

(a) Flatwise bending moment

Harmonic number	Experimental		MOSTAS-A		MOSTAS-B	
	Amp, ft-lb	Phase, deg	Amp, ft-lb	Phase, deg	Amp, ft-lb	Phase, deg
0	35 400	0	37 490	0	35 770	0
1	31 200	24	35 920	22	38 030	20
2	25 700	23	17 240	19	17 170	19
3	17 400	-38	36 250	20	51 150	67
4	7 100	-70	9 848	139	10 730	130
5	7 800	-113	50 300	147	15 470	-141
6	3 000	-126	1 649	178	1 722	-179

(b) Edgewise bending moment

0	-20 900	0	-16 880	0	-24 510	0
1	42 500	-2	36 790	88	37 990	85
2	5 200	160	2 882	-156	1 100	-55
3	11 600	-12	8 196	58	12 620	64
4	2 400	144	2 186	-87	10 350	68
5	13 800	109	1 505	-92	15 080	-100
6	2 200	-150	1 967	-94	2 509	-94

TABLE 3. - ROTOR BLADE PROPERTIES

Spanwise location, ft	Blade chord, ft	Blade twist, rad	Distributed mass, slug/ft	Mode 1		Mode 2	
				Edgewise deflection, ft/rad	Flatwise deflection, ft/rad	Edgewise deflection, ft/rad	Flatwise deflection, ft/rad
0	0	0	0	0	0	0	0
3.33	0	0	0	.0024	-.0111	-.0415	-.0064
4.00	4.5	.556	0	.0045	-.0210	-.0777	-.0120
6.75	4.5	.556	1.4593	.0218	-.0988	-.3558	-.0497
15.63	4.5	.261	.8627	.1914	-.7779	-2.3437	-.1966
25.00	3.925	.119	1.1071	.5924	-2.4824	-6.3133	-.5092
30.83	3.558	.0715	.9678	.9457	-4.1833	-9.6614	-.9097
37.50	3.138	.0346	.8087	1.4202	-6.7544	-14.1638	-1.6545
46.88	2.547	0	.6104	2.1844	-11.7445	-21.5842	-3.4899
50.00	2.35	-.0087	.5778	2.4575	-13.8582	-24.3409	-4.4038
56.25	1.956	-.0233	.3139	3.0171	-18.8374	-30.2452	-6.8061
59.38	1.759	-.0294	.2961	3.2928	-21.8434	-33.3369	-8.4313
62.50	1.563	-.0349	.2664	3.5673	-24.9446	-36.457	-10.1432
	frequency, rps			11.98		17.76	

TABLE 4. - POWER TRAIN PROPERTIES

Parameter	Values			
Element no.	1	2	3	4
J, slug-ft^2	615.8	938.4	1.22	1.408
K, ft-lb/rad	9.8×10^6	9.8×10^6	5.55×10^4	2.36×10^4
B, ft-lb sec/rad	388	480	1.30	0.91
C, ft-lb sec/rad	766	960	2.6	1.82

TABLE 5. - POD PROPERTIES FOR MOD-0 WIND TURBINE

(a) Pod mass and inertias

Mass, slug	I_{xx}, slug-ft^2	I_{yy}, slug-ft^2	I_{zz}, slug-ft^2
1118	5000	78600	78600

(b) Nonzero values of symmetric pod stiffness matrix

Value	Matrix position - row, column					
-1.2×10^6	2,8	3,9	8,14	9,15		
1.2×10^6	2,2	3,3	14,14	15,15		
-6.0×10^8	3,5	3,11	6,8	9,17	12,14	14,18
6.0×10^8	6,2	5,9	8,18	11,15	15,17	
-7.5×10^8	7,19	8,20				
7.5×10^8	19,19	20,20				
9.9×10^8	8,8					
-1.0×10^9	1,7	9,21				
1.0×10^9	1,1	13,13	21,21			
1.24×10^9	9,9					
-1.5×10^9	8,10	8,22	11,19	19,23		
1.5×10^9	7,11	7,23	10,20	20,22		
2.0×10^9	5,11	6,12	10,22	11,17	11,23	12,18
2.75×10^9	7,7					
4.0×10^9	5,5	6,6	17,17	18,18	22,22	23,23
-1.0×10^{10}	4,10	7,13	10,16	12,24		
1.0×10^{10}	4,4	16,16	24,24			
1.2×10^{10}	11,11					
1.8×10^{10}	12,12					
2.4×10^{10}	10,10					

(c) Yaw drive system stiffnesses

Shear and compression	1.0×10^8 lb/ft
Bending	1.0×10^8 ft-lb/rad
Torsional (Yaw)	0-1.0×10^{12} ft-lb/rad

(d) Yaw drive stiffnesses for experimental data cases

Yaw drive configuration	Free	Single	Dual (no preload)	Dual (preload)[a]	Fixed
Stiffness, ft-lb/rad	0.0	7.91×10^6	15.81×10^6	22.35×10^6	1.0×10^{12}

[a]30 000 lb-in.

TABLE 6. - TOWER PROPERTIES

			Mode 1		Mode 2		Mode 3
Height, ft	Mass, slug	Torsional inertia, slug-ft^2	Fore/aft deflection, ft	Pitch rotation, rad	Lateral deflection, ft	Roll rotation, rad	Yaw rotation, rad
0	186.6	0	0	0	0	0	0
21.	330.0	0	.0241	-.0022	.0245	.00224	.0898
38.	266.18	66100	.0901	-.00542	.0916	.00551	.261
54.	220.96	23800	.216	-.0101	.219	.0102	.347
68.	177.2	13200	.394	-.0149	.398	.0150	.460
80.92	203.26	7660	.623	-.0201	.628	.0200	.644
93	160.03	5900	.905	-.0258	.907	.0252	.916
96.67	35.78	2480	1.0	-.0259	1.0	.0254	1.0
Frequency, Hz			2.18		2.22		3.75
Generalized mass			1483 slugs		1483 slugs		173 200 slug-ft^2
Generalized stiffness			0.2782×10^6 lb/ft		0.2798×10^6 lb/ft		96.15×10^6 ft-lb/rad

TABLE 7. - COMPARISON OF FREQUENCIES OF FLOQUET THEORY AND APPROXIMATE METHOD FOR HYPOTHETICAL MODEL

Rotational speed	Frequencies from Floquet theory						Approximate method (Eq. (B7) with time-averaged coefficients)		
	Equation (B3)			Equation (B7)					
Ω/ω_ζ	ω_1/ω_ζ	ω_2/ω_ζ	ω_3/ω_ζ	ω_1/ω_ζ	ω_2/ω_ζ	ω_3/ω_ζ	ω_1/ω_ζ	ω_2/ω_ζ	ω_3/ω_ζ
0.2	1.00	0.83	1.01	1.00	0.83	1.01	1.00	2.49	0.92
.4	↓	.70	0.94	↓	.70	0.94	↓	1.16	.87
.6	↓	.53	.92	↓	.53	.92	↓	0.53	.97
.8	↓	.35	.92	↓	.35	.92	↓	.22	.96
1.0	↓	.18	.92	↓	.18	.92	↓	.00	.95
1.2	↓	.01	.91	↓	.01	.91	↓	.18	.96
1.4	↓	.17	.91	↓	.17	.91	↓	.34	.76
1.6	↓	.33	.90	↓	.33	.90	↓	.48	.96
1.8	↓	.50	.90	↓	.50	.90	↓	.60	.98
2.0	↓	.67	.88	↓	.67	.88	↓	.72	1.00
2.2	↓	.85	.85	↓	.85	.85	↓	.80	1.04
2.4	↓	.93	.93	↓	.93	.93	↓	1.11	0.85
2.6	↓	1.01	1.01	↓	1.01	1.01	↓	1.20	.88
2.8	↓	1.20	0.96	↓	1.20	0.96	↓	1.31	.89
3.0	↓	1.36	0.94	↓	1.36	0.94	↓	1.41	.90

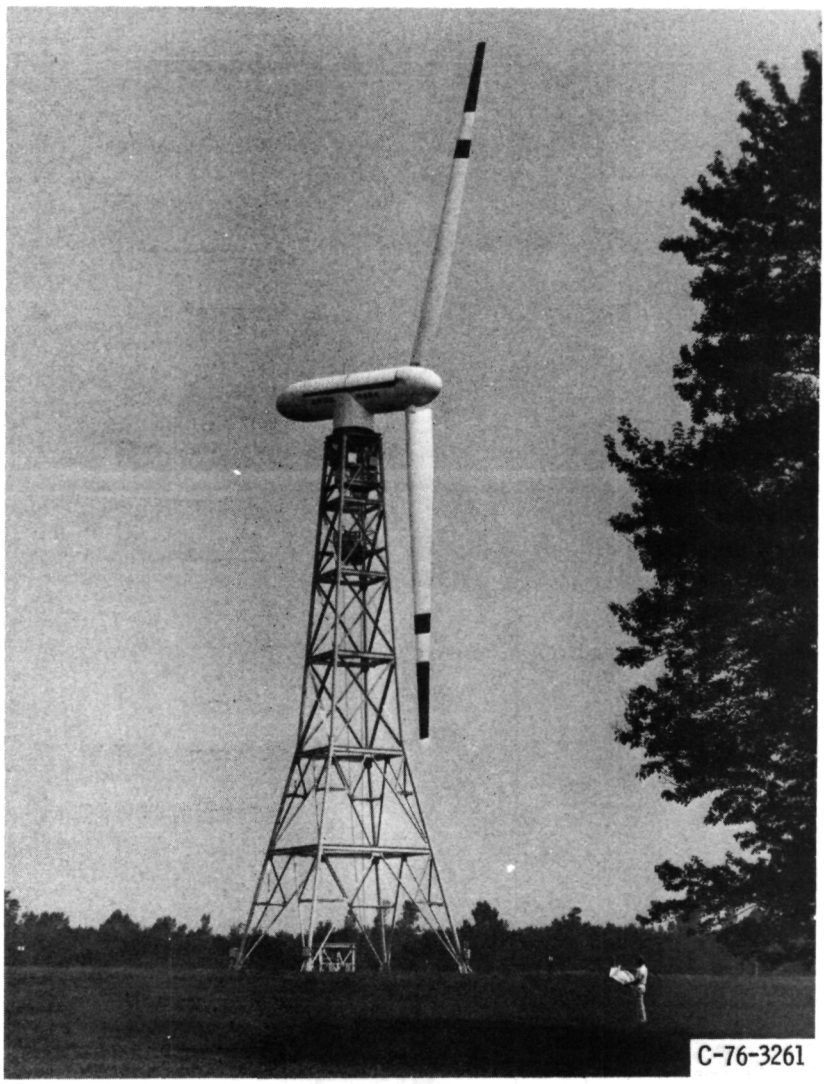

Figure 1. - DOE/NASA 100 kW Mod-0 wind turbine (formally ERDA/NASA).

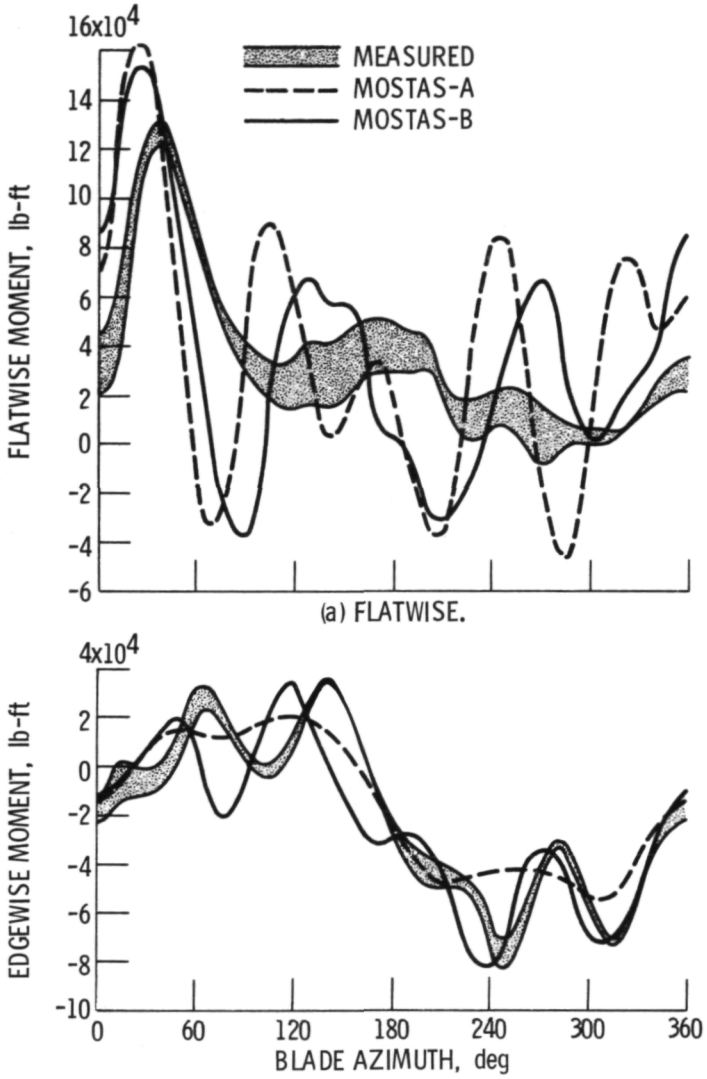

Figure 2. - Comparison of experimental and analytical bending moment time histories for single yaw case (at 5% blade span).

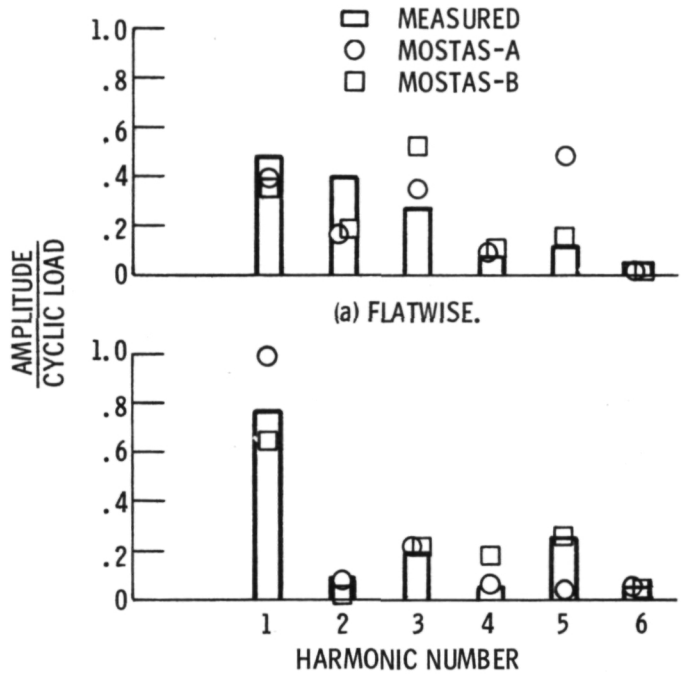

Figure 3. - Comparison of measured and calculated harmonic contents of moment load cycles.

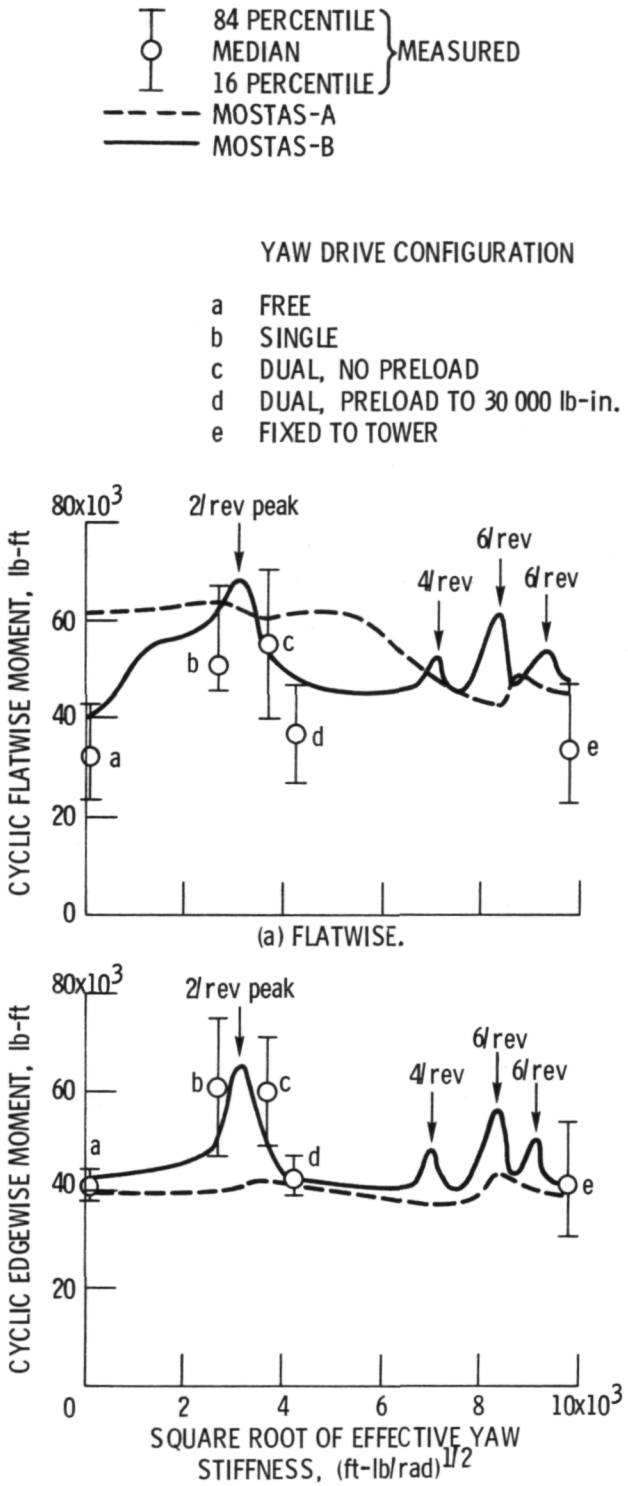

Figure 4. - Comparison of experimental and analytical cyclic bending moment for the Mod-0 wind turbine (at 5% blade span).

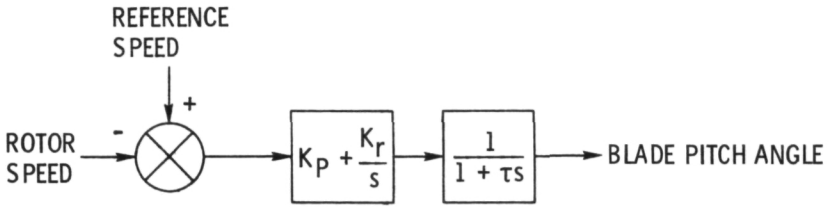

CONTROLLER ACTUATOR

PROPORTIONAL GAIN, $K_P = 0.0$
INTEGRAL GAIN, $K_r = 0.03\ sec^2$
TIME CONSTANT, $\tau = 100.0\ sec^{-1}$
LAPLACE VARIABLE, s

(a) PITCH CONTROL SCHEMATIC.

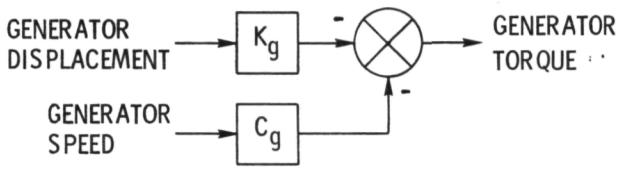

EQUIVALENT STIFFNESS, $K_g = 1260$ ft-lb/rad
EQUIVALENT DAMPING, $C_g = 20$ ft-lb sec/rad

(b) GENERATOR SCHEMATIC.

Figure 5. - Control system model of Mod-0 wind turbine.

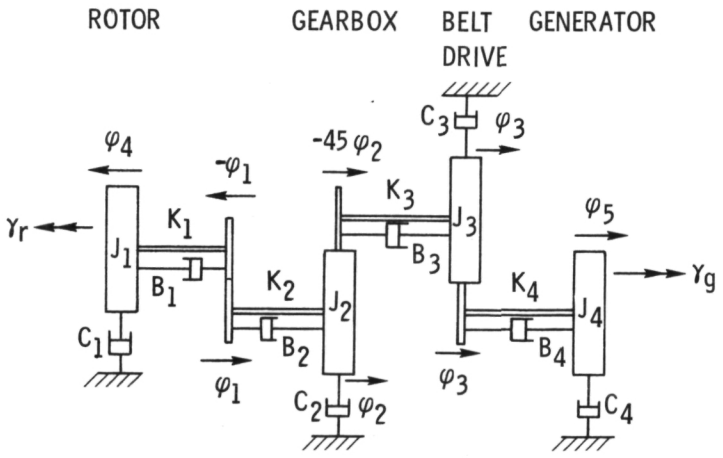

Figure 6. - Schematic for power train model of Mod-0 wind turbine.

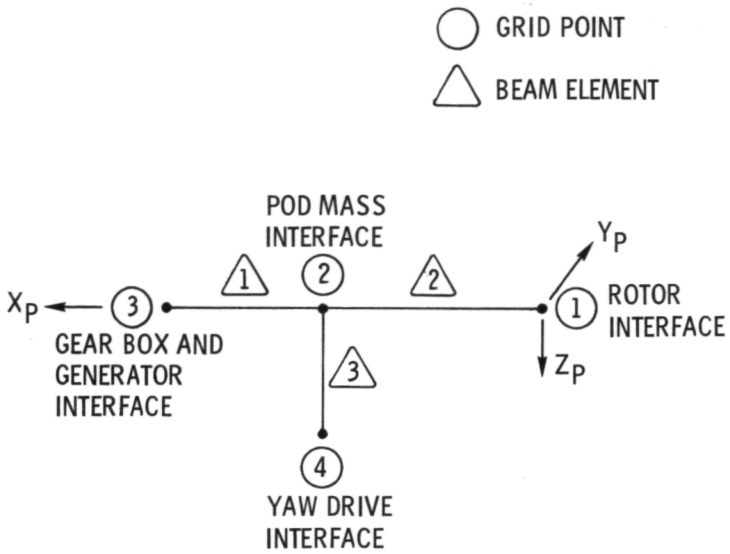

Figure 7. - Schematic for pod model of Mod-0 wind turbine.

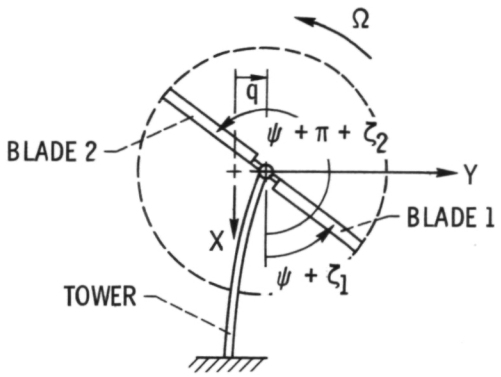

Figure 8. - Hypothetical three-degree of freedom model (q is tower lateral motion, ζ_1 and ζ_2 are lead-lag motions of blades 1 and 2, respectively).

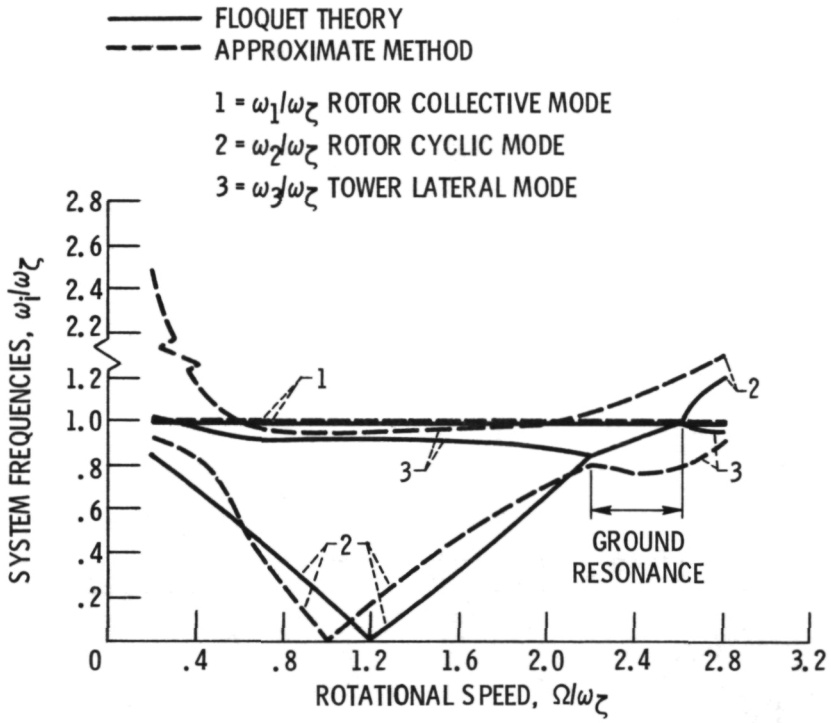

Figure 9. - Variation of frequencies with rotational speed of a three-degree of freedom hypothetical model - tower lateral to lead-lag frequency ratio, $\omega_t/\omega_\zeta = 0.924$, $S/M_tR = 0.0693$, $SR/I = 1.84$.

1. Report No. NASA TM-79101	2. Government Accession No.	3. Recipient's Catalog No.
4. Title and Subtitle EVALUATION OF MOSTAS COMPUTER CODE FOR PREDICTING DYNAMIC LOADS IN TWO-BLADED WIND TURBINES		5. Report Date 6. Performing Organization Code
7. Author(s) K. R. V. Kaza, The University of Toledo; and D. C. Janetzke and T. L. Sullivan, Lewis Research Center		8. Performing Organization Report No. E-9925 10. Work Unit No.
9. Performing Organization Name and Address National Aeronautics and Space Administration Lewis Research Center Cleveland, Ohio 44135		11. Contract or Grant No. 13. Type of Report and Period Covered Technical Memorandum
12. Sponsoring Agency Name and Address U.S. Department of Energy Division of Distributed Solar Technology Washington, D.C. 20545		14. Sponsoring Agency ~~Code~~ Report No. DOE/NASA/1028-79/2

15. Supplementary Notes

Prepared under Interagency Agreement E(49-26)-1028. To be presented at AIAA/ASME/ASCE/AHS Twentieth Structures, Structural Dynamics, and Materials Conference, St. Louis, Missouri, April 4-6, 1979.

16. Abstract

Calculated dynamic blade loads are compared with measured loads over a range of yaw stiffnesses of the DOE/NASA Mod-0 wind turbine to evaluate the performance of two versions of the MOSTAS computer code. The first version uses a time-averaged coefficient approximation in conjunction with a multiblade coordinate transformation for two-bladed rotors to solve the equations of motion by standard eigenanalysis. The results obtained with this approximate analysis do not agree with dynamic blade load amplifications at or close to resonance conditions. The results of the second version, which accounts for periodic coefficients while solving the equations by a time history integration, compare well with the measured data. To explain the deficiencies of the first version and to examine the validity of the transformation, an investigation was made with the aid of a hypothetical three-degree of freedom dynamic model. The exact equations of motion of this model were solved using the Floquet-Lipunov method both before and after applying the transformation. Next, the equations with time-averaged coefficients after applying the transformation were solved by standard eigenanalysis. It was found that the transformation is valid but the associated time-averaged coefficient approximation is inadequate for dynamic analysis of two-bladed rotors.

17. Key Words (Suggested by Author(s))	18. Distribution Statement
Wind turbine Dynamic response Dynamic stability Two-bladed rotors	Unclassified - unlimited STAR Category 44 DOE Category UC-60

19. Security Classif. (of this report)	20. Security Classif. (of this page)	21. No. of Pages	22. Price*
Unclassified	Unclassified		

* For sale by the National Technical Information Service, Springfield, Virginia 22161